



Understanding the role of anthropogenic emissions in glaciers retreat in the central Andes of Chile

Francisco Cereceda-Balic^{a,b,*}, Maria F. Ruggeri^a, Víctor Vidal^{a,b}, Lucas Ruiz^c, Joshua S. Fu^d

^a Centre for Environmental Technologies, Universidad Técnica Federico Santa María, Valparaíso, Chile

^b Department of Chemistry, Universidad Técnica Federico Santa María, Valparaíso, Chile

^c Instituto Argentino de Nivología, Glaciología y Ciencias Ambientales (IANIGLA), Gobierno de Mendoza, Universidad Nacional de Cuyo, CONICET, Mendoza, Argentina

^d Department of Civil and Environmental Engineering, University of Tennessee, Knoxville, USA

ARTICLE INFO

Keywords:

Black carbon
Glacier mass balance
Snow chemistry
Albedo
Climate change v/s anthropogenic impact

ABSTRACT

Glaciers in Chilean Central Andes have significantly retreated, at least, in the last 60 years. From 2004 to 2014, the largest retreat in the area ($-0.15 \text{ km}^2 \text{ yr}^{-1}$) was observed at Olivares Alpha Glacier (OAG). Previous glacier fluctuation studies proposed that two open-pit mines distant 7 km from the glacier could be the cause of its enhanced retreat. However, this had not been yet tested due to the lack of measured data. Here, we investigated the impact that major air pollutants emitted by local mining activities could have on the differences observed in OAG glacial retreat compared with a glacier of similar size and altitude with no nearby anthropogenic sources: Bello Glacier (BG), which has a reported lower retreat ($-0.02 \text{ km}^2 \text{ yr}^{-1}$). Results revealed a link between anthropogenic air pollutants and glacial retreat rates, meaning that glacial retreat is decoupled from climatic and glaciological factors. Considering that both glaciers are located in the same climatic setting, the anthropogenic air pollutants deposited onto the OAG surface appear to be forcing positive feedback in which the pollutants deposition best explain the differences in the glacier retreat. With the results of this study, it has been calculated that the impact of mining in OAG could be responsible for 82% of its total retreat since between 2004 and 2014, and only the remaining 18% would correspond to the impact of climate change.

1. Introduction

Scientific evidence indicates that the Andes cryosphere has responded strongly to climate change through retreat of its glaciers, which have major implications for the availability of water resources in the short term (Molina et al., 2015). These water reservoirs help to mitigate the negative impacts from droughts by guaranteeing the main freshwater source to downstream communities (Masiokas et al., 2020). In this context, the case of Chile is of great concern, since it has the largest portion of the Andean cryosphere: More than 90 glaciers (116 km^2) in the northern zone; 1320 glaciers in the Central Andes (900 km^2); about 300 glaciers in the southern zone (400 km^2). In Chilean Patagonia there are around of $20,000 \text{ km}^2$ of ice cover, where Southern Ice Field is the second largest mass of extra-polar ice in the world. Specifically in the Chilean Central Andes (ChiCA) (32° – 36° S), different studies agree that glaciers in this zone have retreated since, at least, 1955 (Ayala et al., 2016, 2020; Baraza et al., 2017; DGA, 2010; Dirección General de Aguas, 2011; Farías-Barahona et al., 2019; Malmros et al., 2016).

Climate conditions in this area are semi-arid and Mediterranean (Shaw et al., 2020). Precipitation occurs mostly during austral winters and its amount is strongly influenced by the “El Niño Southern Oscillation” (ENSO) (Malmros et al., 2018). Above this interannual variability, a precipitation decline has been observed in the area since the 1970s. Particularly since 2010, there has been a sequence of dry years which has been called Mega Drought (Garreaud et al., 2020). Boisier et al. (2016) estimated that a quarter of this event is attributable to anthropogenic climate change. In addition, a warming of $\sim +0.25^\circ\text{C}$ per decade was detected (Farías-Barahona et al., 2019). Dussaillant et al. (2019) have shown that, over this region, there has been a recent drastic glacier loss coincident with the Mega Drought. Numerous recent works (Ayala et al., 2020; Baraza et al., 2017; Farías-Barahona et al., 2020; Malmros et al., 2016; Ruiz Pereira and Veetil, 2019; Shaw et al., 2020), reported strong differences in the retreat among glaciers of the ChiCA, and they agreed that these differences cannot be fully explained from the climatic and glaciological aspects. In this sense, several studies (Ayala et al., 2020; Bellisario et al., 2013; Farías-Barahona et al., 2020;

* Corresponding author. Centre for Environmental Technologies, Universidad Técnica Federico Santa María, Valparaíso, Chile.
E-mail address: francisco.cereceda@usm.cl (F. Cereceda-Balic).

Malmros et al., 2016; Ruiz Pereira and Veetil, 2019) explicitly mentioned that the significant reduction in some glaciers of the area could be due to the deposition of absorbing substances emitted from open-pit copper mines located in its vicinity (Figure S1), but so far this has not been proven.

To understand the reason, aerosols generated by different emitting sources that are prone to be transported through the atmosphere and deposited over glacier and snow-covered areas became our focus. Among the numerous substances that constitute these atmospheric aerosols, there are light-absorbing particles (LAPs) that absorb solar energy that produce a decrease in the natural albedo of the snow/ice surfaces and accelerate their melting. Among a variety of LAPs, that also includes Brown Carbon and Mineral Dust, Black Carbon (BC), produced by incomplete combustion of fossil fuels and biomass, is pointed as the main LAP (Bond et al., 2013; Cereceda-Balic et al., 2019; Dumont et al., 2014; Hadley and Kirchstetter, 2012), as has been shown by other reports around the world (Aamaas et al., 2011; Qu et al., 2014; Yasunari et al., 2013). BC absorbs solar energy in a wide range of wavelengths, from the visible to the near-infrared (NIR) sections of the spectrum, but its ability to absorb in the NIR (700–900 nm) (Doherty et al., 2010) differentiate it from other substances, and this feature is often used to measure it, even though there are other available techniques (Petzold et al., 2013). Although BC is the most absorptive impurity per unit mass, it is not the only important LAP in snow. Mineral dust is about a factor of 50 less effective (per unit mass) at reducing snow albedo. However, in some locations, so much dust is deposited into the snow that it becomes the dominant absorber (Doherty et al., 2010). In contrast to BC, dust absorbs stronger at UV and blue wavelengths (300–400 nm) and weaker at the NIR (Doherty et al., 2010). In addition to BC and dust, atmospheric aerosols deposited in snow and ice are constituted by other substances, such as trace metals. Although these do not have absorbent properties, some of them are considered as specific tracers of certain anthropogenic activities (Cereceda-Balic et al., 2012; Jeffries, 1990; Lai et al., 2017; Zdanowicz et al., 2017). However, hitherto, the presence of these aerosols has been studied sparingly in the area (Bolaño-Ortiz et al., 2019; Cereceda-Balic et al., 2019, 2018; 2012; Cereceda-Balic et al., 2019; Molina et al., 2015; Rowe et al., 2019), and its relation with glacier variations has been barely studied (Arenson et al., 2015; Cereceda-Balic et al., 2020).

Regarding a potential impact of pollutants emitted in Santiago de Chile and transported through the atmosphere up to the Andean glaciers, Lapere et al. (2021) found that a plausible winter pattern could be that BC from Santiago is blown towards the southeast cordillera consistently with the afternoon westerlies induced by mountain-valley circulation, being the Andean area located at the southeast of the city the most affected by Santiago's emissions, with no potential transport to the northern slope of the Andes, where OAG is located. Cordova et al. (2016) measured Cloud Condensation Nuclei (CCN) in the ChiCA, in a location southeast of Santiago. They found that during synoptic conditions resulting in clear days at the site, the mesoscale mountain-valley circulation could lead to transporting pollutants upwards during the day in the southern direction, causing diluted particle concentrations beyond the summits of the highest peaks. However, in cloudy days with reduced up-valley circulation, they did not find increased concentrations associated with transport. Besides, they performed a back trajectories analysis, which indicated that air masses reaching the site during the field campaign were seldom influenced by pollution from Santiago.

2. Materials and methods

2.1. Study area

Recent works have highlighted that the largest recession rate in the ChiCA was observed at Olivares Alpha Glacier (OAG) (Ayala et al., 2020; Baraza et al., 2017; Farías-Barahona et al., 2020; Malmros et al., 2016; Ruiz Pereira and Veetil, 2019; Shaw et al., 2020), which presented a

negative glacier mass balance of $-0.62 \text{ m w.e.a}^{-1}$ (Farías-Barahona et al., 2020), losing 63% of its ice area since 1955 (Malmros et al., 2016). OAG (33.19°S ; 70.22°W – 4520 m. a.s.l) is a 3.8 km^2 (2014) glacier located 50 km northeast of Santiago (Fig. 1), in the most glaciated area of the Maipo Basin (Stehlik et al., 2017). Several studies (Ayala et al., 2020; Bellisario et al., 2013; Farías-Barahona et al., 2020; Malmros et al., 2016; Ruiz Pereira and Veetil, 2019) explicitly mentioned that the significant reduction in the OAG could be due to the deposition of absorbing substances emitted from open-pit copper mines located in its vicinity, since OAG is located only 7 km southeast of two open pit mines that are currently operating in the study area (Figure S1), where copper and molybdenum minerals are extracted.

To investigate and quantify the impact that air pollutants emitted by local anthropogenic activities have on the differences observed in the glacier retreat in the ChiCA, Bello Glacier (BG) (33.53°S ; 69.95°W – 4430 m. a.s.l.) (Fig. 1), a size and altitude comparable glacier (Table S1) and logically accessible with no nearby anthropogenic emission sources, has been selected to evaluate the impact of atmospheric pollutants from mines operations may have on OAG. BG is located 65 km east of Santiago and 45 km southeast of OAG (Fig. 1). BG is a 3.6 km^2 (2014) glacier, part of Yeso Basin along with Yeso and Piramide glaciers (Burger et al., 2019), which is of societal importance, since its outflow is a tributary input to the “El Yeso” reservoir, the second reservoir of water for consumption and irrigation in the Santiago Metropolitan Region.

2.2. Analysis of remote sensing images

The area extent of OAG and BG between 2004 and 2014 has been mapped using a combination of semi-automated and manual classification methods and manual delineation over LANDSAT images (Man et al., 2014; Paul et al., 2013).

Landsat scenes (path 233, row 83), with a spatial resolution of 30 m, were downloaded from the United States Geological Survey (USGS), Earth Resources Observation and Science Center (EROS). Landsat images were carefully selected, considering only austral summer periods (December–April), when seasonal snow cover is at a minimum (Malmros et al., 2016). Additionally, images were subjected to visual inspection before being used, to verify the absence of snow as well as cloudiness in the areas of interest. They were orthorectified and projected to the Universal Transverse Mercator (UTM) coordinate system, zone 19 South (Table S1).

The Normalized Difference Snow Index (NDSI) was used (Riggs et al., 1994), to distinguish glacier ice from non-ice areas. For years 2004–2011, the NDSI was calculated from Landsat 5 Thematic Mapper (TM) using TM band 2 (visible green, 0.52–0.60 μm) and TM band 5 (mid-infrared, 1.55–1.75 μm).

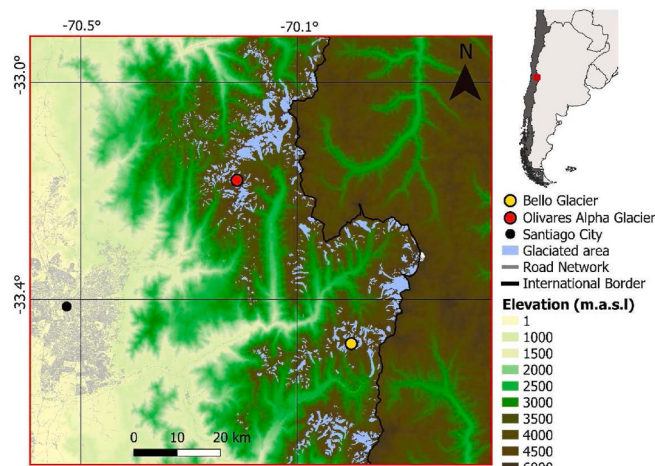


Fig. 1. Study area, with studied glaciers indicated by circles.

Meanwhile, for the years 2013 and 2014, Landsat 8 Thermal Infrared Sensor (OLI-TIRS) images were used. In these cases, because Landsat 8 has a different spectral width for equivalent bands, the visible band 3 instead of band 2, and the infrared band corresponded with band 6 instead of band 5 were used in the calculation of the NDSI. For 2012, the NDSI couldn't be calculated since there were no Landsat images free of seasonal snow and cloud available for that year.

After calculating the NDSI, monoband images were obtained. A threshold value was applied to each image, above which a pixel was considered to be glacial ice, and below which it was not (Riggs et al., 1994). This threshold value was set from the analysis of each image obtained and was conservatively assumed around 0.6. In some cases, manual digitization was applied to the correction of automatically derived outlines. The calculations made on the images as well as the mapping and calculation of the areas for the analyzed years were carried out using the open-source software QGIS v3.4.10.

Finally, it was conservative assumed that uncertainty in the mapping extent of the glaciers at each year is similar to the reported differences between automatically derived outlines from manually digitized outlines, roughly between 2% and 5% of the glacier extent (Fig. 2) (Paul et al., 2013).

2.3. Regional glacier mass balance change (2000–2018)

The mass change of glaciers with more than 0.5 km^2 at less than 100 km from the open pits was analyzed. Glaciers larger than 0.5 km^2 were selected to avoid artifacts or anomalous surface mass balance values due to the un-sampling or noise over smaller glaciers.

The National glacier inventory of Chile and Argentina (Barcaza et al., 2017; Zalazar et al., 2017) in combination with the ASTERIX (ASTER monitoring of Ice towards eXtinction' geodetic method) glacier elevation change dataset from Dussaillant et al. (2019) were used to calculate individual glacier mass balances for a complete period 2000–2018. A total of 301 glaciers were identified with an extent larger than 0.5 km^2 at less than 100 km from the open pits (Fig. 3).

Dussaillant et al. (2019) calculated the glacier volume changes for the Southern Andes using time series of digital elevation models (DEMs) obtained from Advanced Spaceborne Thermal Emission and Reflection Radiometer (ASTER) stereo images. The reader is referred to the original publication for more details in the methodology and uncertainty assessment of the ASTERIX dataset used here.

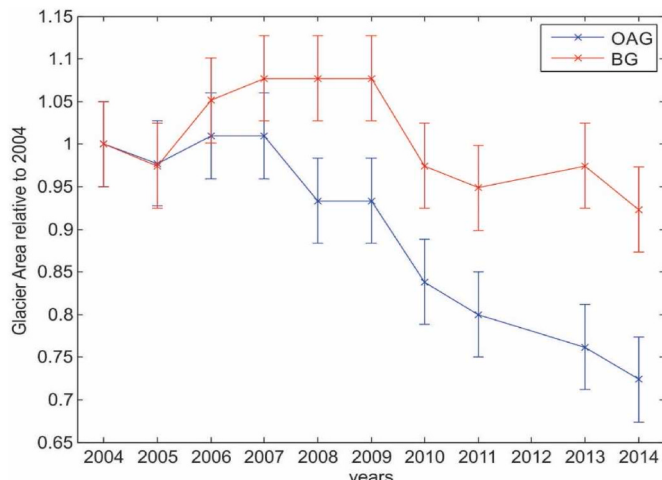


Fig. 2. Relative area changes of OAG (blue line) and BG (red line) between 2004 and 2014. Error bars shown an uncertainty of 5% in the extent of the glacier at each particular year, based on estimations of Paul et al. (2013). (For interpretation of the references to color in this figure legend, the reader is referred to the Web version of this article.)

The volume change for each glacier was calculated following the approach of Ruiz et al. (2017). Elevation changes were analyzed for 50 m altitude bands. Within each altitude band, elevation changes were averaged after excluding pixels for which absolute height differences differed by more than three standard deviations from the mean (Berthier et al., 2004). There were no data (gaps in Dussaillant grids) for those altitude bands, an interpolation scheme was used to derive the elevation change at that elevation bin. If the bins with no data were located close to the maximum height of the glaciers a nearest-neighbor interpolation method was used to maintain the same pattern of elevation change with elevation observed in the rest of the glacier. For those bins with no data located in the middle or in the snout of the glaciers, a linear interpolation method was used. The conversion of elevation change to mass balance requires knowledge of the density of the material that has been lost or gained and its evolution during the study period. Given the lack of measurements of density profiles over the entire snow/firn/ice column in analyzed glaciers, a constant density conversion factor of $850 \pm 60 \text{ kg m}^{-3}$ was applied (Huss, 2013). The reader is referred to Ruiz et al. (2017) for more details in the methodology and uncertainty assessment used to calculate the surface mass balance of the glaciers used here.

2.4. Atmospheric measurement of PM and BC

PM and BC were determined at OAG and BG by using on-line devices, which were installed directly on the surface of the glaciers and were powered by energy from photovoltaic solar panels and a battery set. The field campaign in BG was held in the period between September 12 and 24, 2014, while in OAG the field campaign was held between October 21 and 29, 2014. Dates, as well as the duration of the field campaigns, were determined by logistical aspects. Snow samples, whose analysis and result are detailed below, were taken during the mentioned dates for each glacier. PM was measured by using an aerosol laser spectrometer Grimm Model EDM 107 (Durag Group, Hamburg, Germany). For this study in Santiago, a monitoring station of the Chilean automated meteorological and air quality monitoring network (SINCA) was used, located in Parque O'Higgins, this station has population representativeness for this city and represents the average air pollution of the capital from Chile. PM were monitored in parallel and in the same dates, throughout the entire period of the glacier monitoring campaigns using an aerosol laser spectrometer Grimm Model 1.109 (Durag Group, Hamburg, Germany). The measurement principle of these devices is light scattering, and the light source is a laser diode. The instrument can be used easily in the field to determine the mass concentration of PM₁, PM_{2.5}, and PM₁₀ and particle size distribution between 0.27 and 34 μm (31 different channels). The sample flow was 1.2 L min^{-1} . Due to extreme weather conditions in glaciers, Grimm EDM 107 equipment was placed inside a Weather Housing Grimm Model EDM 164 (Durag Group, Hamburg, Germany), which accounted for weather sealing and heated sampling probe, to avoid sample condensation.

BC atmospheric concentration in OAG and BG was determined simultaneously with PM, using a microAeth® Model AE51 (Aethlabs, CA, USA). The measurement principle is the rate of change in absorption ($\lambda: 880 \text{ nm}$) of transmitted light in a continuous collection of aerosols deposited on a Teflon-coated borosilicate glass fiber filter. The measurement at 880 nm can be interpreted as BC atmospheric concentration. The sample flow was 150 mL min^{-1} . Data of PM and BC were taken continuously every 1 min. BC atmospheric concentration in Santiago was measured in parallel with glacier campaigns using a Multi-angle Absorption Photometer Model 5012 (MAAP) (Thermo Scientific, USA), a filter-based instrument that measures atmospheric BC concentration at the wavelength of 637 nm. The airflow (fixed in $1.0 \text{ m}^3 \text{ h}^{-1}$) was measured continuously by the pressure drop across an orifice, and the filter tape was moved automatically forward to the next blank sampling spot when transmission of the particle-loaded spot decreased below 20%.

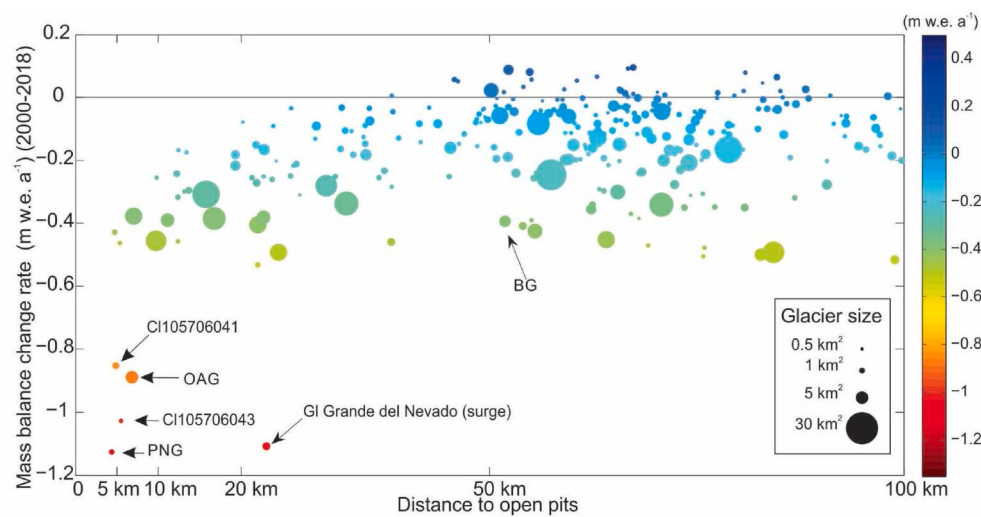


Fig. 3. Surface mass balance rate of glaciers (larger than 0.5 km^2) close to the open pits (less than 100 km). Dot size is proportional to the glacier extent. Glaciers that presented the most negative mass balance in the area are closer to the open pit. Olivares Alpha Glacier (OAG), Bello Glacier (BG), Paloma Norte Glacier (PNG), Grande del Nevado Glacier and other two glaciers (identified with their ID in the Glacier Inventory of Chile (Barcaza et al., 2017) close to the open pit are highlighted.

2.5. Measurement of meteorological variables and albedo

Meteorological data were recorded every 1 min in the same dates that PM and BC in each glacier, by using a HOBO U30 weather monitoring station (Onset Computer Corporation, MA, USA). In OAG the station was located at $33^\circ 11' 33.42''\text{S}$ - $70^\circ 13' 16.91''\text{O}$ (latitude-longitude), altitude: 4470 masl, while in BG it was located at $33^\circ 31' 56.9''\text{S}$ - $69^\circ 56' 54.73''\text{W}$ (latitude-longitude), altitude: 4290 masl. In Santiago, the meteorology was obtained from the air quality monitoring station of Parque O'Higgins, located at $33^\circ 27' 50.96''\text{S}$ - $70^\circ 39' 38.75''\text{W}$ (latitude-longitude), altitude: 530 masl, belonging to "SINCA". Temperature and relative humidity were measured with an Onset S-THB M002 sensor, and the barometric pressure was measured with an Onset S-BPB-CM50 sensor. Wind speed and direction were measured with Onset S-WSB-M003 and S-WDA-M003 sensors, respectively. Hourly means were extracted for further analysis. A special treatment was applied to calculate hourly averaged Wind Direction (WD) since this variable was reported as an angle in degrees, 0° - 360° , where 0° and 360° represents a wind blowing from a northerly direction, so the arithmetic mean cannot be calculated because it induces a numerical error. To deal with this scale discontinuity, trigonometric functions were used to correctly handle wind as a vector instead of a scalar variable (Grange, 2015).

Snow albedo was determined by calculating the energy balance between incoming short-wave radiation versus surface-reflected short-wave radiation, measured using a portable net radiometer Model CNR4 (Kipp & Zonen, Netherlands), located together with the meteorological station in the same dates, in each glacier. The radiometer included a pyranometer pair, one facing upward, the other facing downward (with sensitivity from 5 to $20 \mu\text{V} (\text{W m}^{-2})^{-1}$), covering the solar spectral range from 300 to 2800 nm (short wave) and a pyrgeometer pair, with a similar configuration than pyranometer pair, (with sensitivity from 5 to $15 \mu\text{V} (\text{W m}^{-2})^{-1}$), covering the thermal infrared spectral range from 4500 to 42,000 nm (long wave). Data from CNR4 was stored every 1 min in a datalogger Logbox SD (Kipp & Zonen, Delft, Netherlands). It must be considered that the accuracy of radiometers is low for low solar elevations (Cereceda-Balic et al., 2018). In consequence, the albedo was analyzed between 11:00 a.m. and 16:00 p.m.

2.6. Snow sampling and analysis

Snow samples were collected in OAG and BG at early spring, during BC, PM, meteorological data and albedo measurements campaigns

(September 2014 in BG and October 2014 in OAG), when precipitations and particulate matter deposition are at their minimum (Vicuña et al., 2011) and when the snowpack reaches its maximum depth before the onset of spring snowmelt. Snow samples were analyzed to determine BC, dust and trace metals concentrations, as is detailed below. Snow samples were collected in Whirl-Pak (Nasco) plastics bags from the top of the snowpack, in an area of 1 m^2 and 5 cm thick layer, using a clean plastic shovel and disposable dust-free nitrile gloves. Samples were taken in three different sites of each glacier (named S1, S2 and S3), in triplicate in each site. Each sample weighed around 1200–1500 g, and they were kept always frozen (-20°C), during transport and storage, until they could be processed. All sampling materials were washed using acid to avoid contamination according to the procedure published by Cereceda-Balic et al. (2012).

Trace elements (Al, As, Cd, Cr, Cu, Fe, Hg, Sb, Pb, and Zn) were determined by Inductively Coupled Plasma Mass Spectrometry (ICP-MS), using an ICP-MS ELAN 9000 (PerkinElmer, MA, USA) equipped with Dynamic Reaction Cell (DRC). The method was described previously by Cereceda-Balic et al. (2012). The accuracy of the analytical procedure was checked by using the certified reference material "SPS-SW2: Reference material for measurements of elements in surface waters", (Spectrapure Standards, Oslo, Norway) (SM). All analyses were performed in triplicate (see S5, and Table S4).

Dust concentration in snow samples from OAG and BG was determined by using a gravimetric method, where snow samples were microwave-assisted melted, then filtered through a specially designed filtration system able to generate a uniform spot on previously weighted Nuclepore 47 mm polycarbonate filters (Cereceda-Balic et al., 2019). After filtration, filters were allowed to dry and weighted again. Dust deposited in filters was determined by weight difference. BC mass concentration in snow was determined in the same filters where dust was measured, through optical attenuation measurements by using a SootScan™, Model OT21 Optical Transmissometer (Magee Scientific; Berkeley, CA, USA), where the optical transmission was compared between the sample and a reference blank filter at 880 nm, following the procedure described in Cereceda-Balic et al. (2019). Attenuation units were converted to BC mass concentration by considering a mass attenuation cross section (MAC) of $4.69 \text{ m}^2 \text{ g}^{-1}$ in equations presented in Cereceda-Balic et al. (2019). This MAC value was obtained by using the MAC presented by Hadley and Kirchstetter (2012) ($7.5 \text{ m}^2 \text{ g}^{-1}$ at 550 nm) for BC in snow, scaled to 880 nm.

2.7. Forward trajectories modeling

HYSPLIT model has been developed by the NOAA Air Resources Laboratory (https://www.ready.noaa.gov/HYSPLIT_traj.php). It was run in the ensemble forward trajectories mode and calculations were made using the GDAS (Global Data Assimilation System) meteorological data with the 0.5-degree archive from the National Center for Environmental Prediction (NCEP), for 24 h duration, for each day of field sampling, starting in BG (September 12 to 21, 2014) and OAG (October 21 to 29, 2014). Besides, forward 24 h trajectories originated in Santiago City were modeled for the sampling periods in both glaciers previously mentioned, in order to elucidate if during those periods BC and PM emissions from Santiago could reach the glaciers.

3. Results and discussion

3.1. Glacier retreat

OAG showed a marked net decrease in its area (-1.45 km^2) between 2004 and 2014, corresponding to 27.6% of its area in 2004. In contrast, BG presented a smaller area reduction (-0.2 km^2) between 2004 and 2014, which means a reduction of 5.1% of its area in 2004. The area change rate has not been constant throughout the period. Between 2004 and 2009, BG experienced an increase in area (7%) meanwhile OAG experience a decrease (-7%). After 2009, both glaciers showed a decrease in their area, being 2010 the year in which this loss was more severe for both. It should be noted that none of the analyzed years presented the opposite trend (Fig. 2, Figure S2, Table S2). These results are in agreement with elevation changes (m a^{-1}) calculated by Farias Barahona et al. (Farías-Barahona et al., 2020), who found that the BG retraction occurred almost completely in the 2010–2015 period, coinciding with the mega-drought in the area, manifesting the strong impact of the climatic component on it. In turn, these authors also found that variations in the OAG have been sustained at least since 1955, by which time the mines in the area were already operational, denoting the effects of mining activity historically and with a dependency that is not exclusive to climatic conditions.

In addition to the area changes previously analyzed, individual glacier mass balance for a complete period 2000–2018 was performed. The mean mass balance rate of all the considered glaciers between 2000 and 2018 was $-0.15 \pm 0.2 \text{ m w. e. a}^{-1}$ (meter of water equivalent per year/annual; \pm one sigma). OAG presented a mass balance rate of $-0.8 \text{ m w. e. a}^{-1}$ meanwhile BG had a mass balance rate of $-0.4 \text{ m w. e. a}^{-1}$. Fig. 3 shows the mass balance rate of the different glaciers sorted by increasing distance from the open pits. Glaciers closer to the open pits had the most negative mass balance. The mean mass balance rate of glaciers at less than 5 km from the open pits was $-0.71 \text{ m w. e. a}^{-1}$, meanwhile those who are between 5 km and 100 km had a mean mass balance of $-0.15 \text{ m w. e. a}^{-1}$. Particularly, the Paloma Norte glacier (PNG) is the one with the most negative mass balance $-1.12 \text{ m w. e. a}^{-1}$ and also the closest to the open pits. Another glacier that presented a strongly negative mass balance ($-1.1 \text{ m w. e. a}^{-1}$) was Grande del Nevado Glacier (GNG), which is a surging glacier (Espízua and Bengoechea, 1990). A surging glacier oscillates between long periods (tens to hundreds of years) of slow flow and shorter periods of typically 10–1000 times faster flow. During the last surge event (2003–2007) GNG front advance roughly 3.7 km (Pitte et al., 2016), increasing considerably its ablation area due to the large volume of ice is transported down the valley. After the surge event, the increased ablation area cause a negative perturbation of the mass budget (Oerlemans and van Pelt, 2015), which was reflected in its strong negative mass balance. Fig. 3 highlights that OAG and PNG and the other two glaciers close to the open pit showed a markedly different behavior from the rest of the glaciers considered in the area, including the BG, which showed a behavior comparable to the rest. This statement agrees with the area change analysis of BG and OAG, presented in this study.

3.2. Field measurements

In order to elucidate the extent to which anthropogenic air pollutants can affect the explored glacier behavior, atmospheric particulate matter (PM), BC concentrations in air and snow, dust and metals in snow, and broadband albedo were measured. Concentrations of measured atmospheric BC showed average values of 108 ng m^{-3} in BG and 294 ng m^{-3} in OAG during the monitoring periods. Fig. 4 shows that atmospheric BC concentration in OAG presented a daily cycle during the first five sampling days (from 21 to 26 of October), increasing between 12 and 20 h. During these days, air temperature showed a similar daily cycle, with maximum values also reached during daylight hours. This potential correlation between air temperature and BC atmospheric levels in OAG may be because, when the temperature increases, the height of the boundary layer also does, providing a pathway for the pollutants generated by the nearby sources to reach a greater height in the atmosphere and be transported to the surface of the OAG. This process allowed airmasses to overcome the physical barriers of the summits of the mountains that separate the open-pit mine from the glacier and overcome the physical barriers they entail.

Wind direction (WD) also presented a marked pattern during day hours in those dates, coming mainly from W and NW (270° – 320°), where mines are located. From day 6 (October 27), BC concentration decreased. The same profile could be seen in air temperature, reinforcing the hypothesis raised previously. Also, during the last sampling days, the wind speed was higher and wind direction was less variable and came mainly from S and SW (160° – 270°), where Santiago City is located, suggesting that levels of BC did not come from local sources generated in the open-pit mine during these days, when they showed to be lower. In Fig. 5 can be seen that in BG, daily cycles of BC concentration and air temperature were not so clear. In BG, winds came mainly from southern directions (100° – 200°), where no emission sources are located, which could explain the lower levels of atmospheric BC than in OAG. Most likely these levels of BC represent the background concentration of this area of the Andes Mountain.

To establish whether the differences observed in BC atmospheric concentrations in OAG and BG are significant, the values observed in both glaciers were subjected to statistical non-parametrical tests of Kolmogorov-Smirnov (Figure S3). According to the statistical tests performed, the atmospheric concentration of BC observed in the OAG is significantly different and higher than that observed in the BG. Considering that both glaciers are at a similar distance from Santiago, it could be considered that another source is significantly influencing OAG, which can be the mining activities, as combustion of diesel machinery and heavy diesel trucks used there (Figure S1).

Snow albedo at both glaciers was determined by calculating the energy balance between incoming short-wave radiation versus surface-reflected short-wave radiation, measured using a portable net radiometer Model CNR4 (Kipp & Zonen, Delft, Netherlands). These measurements exhibited differences between the studied glaciers. The BG presented generally high levels of albedo (Figure S4, A, and B), with an average value of 0.74, reaching maximum in the early afternoon. On the other hand, in the OAG, comparatively lower values were observed (Figure S4, C, and D), with an average of 0.61 where the maximum levels were reached in the morning or midday hours. Considering similarities of both glaciers regarding climatic conditions, the observed albedo differences among them would be due to the differences in LAPs deposition, as it is exposed below.

3.3. Determinations in snow

LAPs content in snow (dust and BC) was determined by triplicate in each glacier (Fig. 6 and Table S3). Dust mass concentration in snow shown to be $153.0 \pm 48.5 \text{ mg kg}^{-1}$ in OAG and $2.3 \pm 0.7 \text{ mg kg}^{-1}$ in BG, meaning that dust concentration in snow from OAG was 67 times higher than those found in BG (Fig. 6). BC mass concentration presented a mean

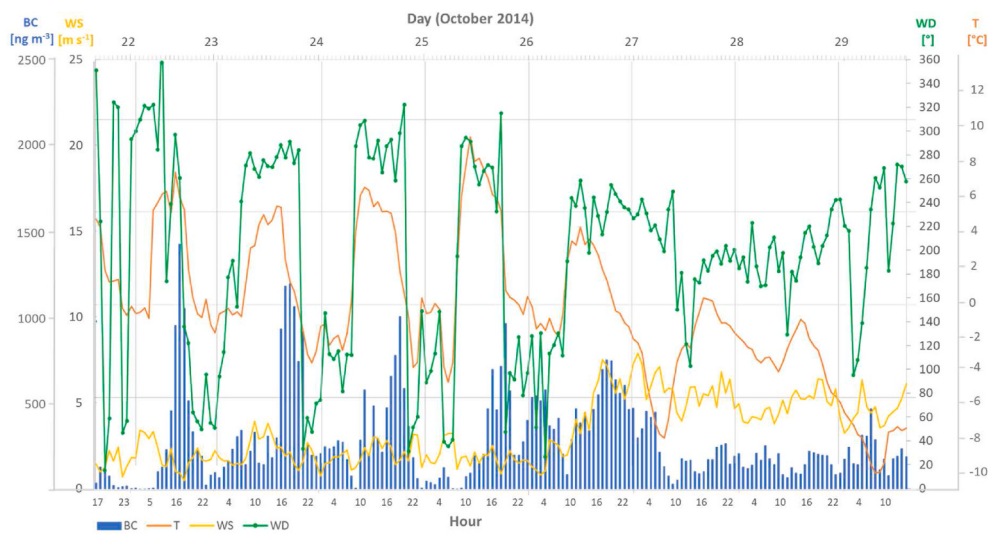


Fig. 4. Hourly-averaged values of Black Carbon concentration (ng m^{-3} , blue bars), wind direction ($^{\circ}$, green dotted line), wind speed (m s^{-1} , yellow line) and air temperature ($^{\circ}\text{C}$, orange line) for each sampling day in OAG. Each variable is represented on a different vertical axis. (For interpretation of the references to color in this figure legend, the reader is referred to the Web version of this article.)

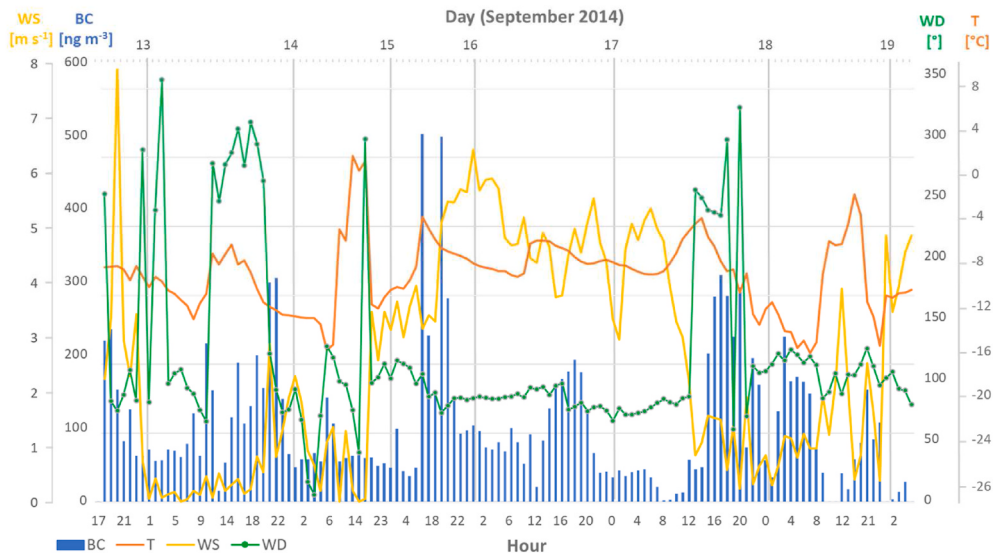


Fig. 5. Hourly-averaged values of Black Carbon concentration (ng m^{-3} , blue bars), wind direction ($^{\circ}$, green dotted line), wind speed (m s^{-1} , yellow line) and air temperature ($^{\circ}\text{C}$, orange line) for each sampling day in BG. Each variable is represented on a different vertical axis. (For interpretation of the references to color in this figure legend, the reader is referred to the Web version of this article.)

value of $1611.9 \pm 455.7 \text{ ng g}^{-1}$ in OAG and $26.3 \pm 5.0 \text{ ng g}^{-1}$ in BG, meaning that BC concentration in snow from OAG was 61 times higher than in BG (Table 1, Fig. 6). In comparison with BC mass concentrations measured in other locations (Table 1), values found in BG showed to be in the same order of magnitude of weak anthropogenic-influenced sites, as measurements performed in some places of North America (Skiles and Painter, 2017), the French Alps (Tuzet et al., 2020), and other sites of the Chilean Andes (Rowe et al., 2019). In contrast, levels of BC measured in the snow from OAG seemed to be in the order of magnitude of those registered in snowy places with a higher degree of anthropic disturbances, as some places in the Tibetan plateau (Zhang et al., 2017) or crowded places of Antarctica (Casey et al., 2017). These findings clearly evidence that the impact of LAPs in OAG is important, and differences found in dust and BC mass concentration in snow, together with atmospheric BC levels, are in keeping with the significant differences found in albedo measurements between OAG and BG.

Also, trace metals concentrations were measured in the surface snow

from OAG and BG, where levels found in the snow of OAG resulted higher than those found in BG snow (Table S5), which in most cases presented values below the limit of detection (<LOD). But quantifying the magnitude of anthropogenic deposition of metals from the atmosphere is not straightforward since metals also occur naturally in soils and rocks and therefore exist even in pristine areas at a background level. To differentiate natural from anthropogenic sources of elements deposited in the snow, and thus to evaluate the contribution of anthropogenic contamination in the receptor area, the enrichment factor (EF) of trace elements was calculated (Section S6 of Supplementary Material). Figure S6 shows that Fe presented EFs in the order of the unit in the surface snow from the two glaciers, meaning that natural dust was the mean input of this element. Cu and As were highly enriched in OAG, independently of the reference of elements composition on the soil considered, while in BG those EFs couldn't be calculated because measured concentrations of Cu and As resulted below the limit of detection. As is normally associated with copper in its deposits (De

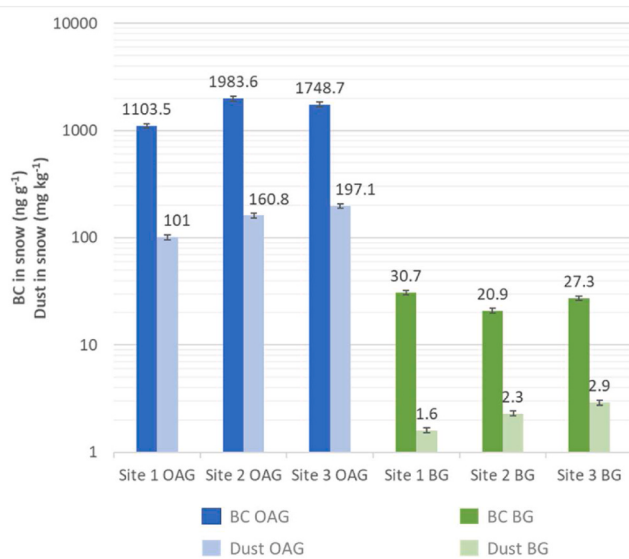


Fig. 6. BC concentration in snow samples (ng g^{-1}) and Dust concentration in snow samples (mg kg^{-1}) obtained in OAG (blue bars) and BG (green bars). Vertical axis is shown in logarithmic units for a better visualization. (For interpretation of the references to color in this figure legend, the reader is referred to the Web version of this article.)

(Gregori et al., 2003), and its high degree of enrichment would be related to the soil disturbance due to mining operations. Pb, a well-known anthropogenic tracer, also resulted enriched in OAG, while in BG it resulted below detection limits. The EF of Zn resulted higher in BG than in OAG, although the level determined in the snow was markedly lower ($3.88 \mu\text{g kg}^{-1}$ in BG vs. $37.97 \mu\text{g kg}^{-1}$ in OAG). This may be because the measured value of Al in the snow from BG (the element used as a reference in Eq. S1 of Supplementary Material) was also much lower than in OAG ($38.45 \mu\text{g kg}^{-1}$ in BG vs. $949.65 \mu\text{g kg}^{-1}$ in OAG). The same occurred with Fe levels, the other soil tracer, which resulted much lower in BG than in OAG. These facts revealed an important impact of mining in OAG not only due to the enrichment of those elements indicated as anthropogenic but also due to the high levels of Al and Fe found. The strong presence of these natural elements in the snow of OAG proves that mining operations release material from soils that reaches nearby glaciers, in keeping with higher dust mass concentrations. These measurements provide strong evidence in linking the effects of mining activity with the dramatic OAG retreat, a fact proposed many times before but being proved here for the first time.

3.4. Is Santiago a main source of atmospheric pollutants for the studied glaciers?

Since both OAG and BG are located in the ChiCA, near Santiago (Chile capital City, 7 million inhabitants), it is important to establish if one of the sources of PM and BC is observed from this city. One antecedent that accounts for the differences between the particulate matter found in both glaciers with respect to the city of Santiago is its size distribution for fine particles (Fig. 7).

Fig. 7 shows that $0.265 \mu\text{m}$ particles presented similar proportions in the BG and OAG (49 and 54% respectively), while in Santiago their percentage reached 37%, on the other hand, $0.375 \mu\text{m}$ particles represented 6 and 5% of the fine fraction of particulate matter in BG and OAG respectively, while in the city of Santiago it reached 13%. These distribution differences allow inferring that the fine particles in the city of Santiago had different sources than the fine particles found in the two glaciers.

Another antecedent that would allow establishing if the contamination by PM and BC observed in both glaciers had similar sources than

Table 1

BC mass concentrations in snow measured in different locations, including those measured in this study. SP2: Single particle incandescence soot photometer. ISSW: Integrating Sphere Integrating SandWich.

| Location | Type of location | BC concentration in snow [ng g^{-1}] | Method used to measure BC | Reference |
|---|---|---|--|---------------------------|
| Olivares Alpha Glacier (OAG), Chilean Central Andes | High Mountain glacier, close to open-pit mines operations | 1611.9 ± 455.7 | Filter-based optical method | This study |
| Bello Glacier (BG), Chilean Central Andes | High Mountain Glacier, control site | 26.3 ± 5.0 | Filter-based optical method | This study |
| Andes of Chile | Different locations of the Andes Mountains of Chile, from latitude 18°S to 41°S | 1–153 | Variety of locations with various techniques, including SP2 and ISSW | Rowe et al. (2019) |
| San Juan Mountains, Colorado, US | Protected site with weak anthropic presence | <1–20 | SP2 | Skiles and Painter (2017) |
| Laohugou No.12 glacier, Tibetan Plateau. | High mountain glacier with influence of atmospheric pollution from urban areas | 1785 ± 326 | Thermal-optical method | Zhang et al. (2017) |
| Col du Lautaret, French Alps | Mountain area with weak anthropic presence | 1–20 | SP2 | Tuzet et al. (2020) |
| Amundsen-Scott South Pole Station, Antarctica | Different sites near the Station, from clean areas to the landing track | 0.1–7000 | SP2 | Casey et al. (2017) |

the city of Santiago is the quantification of the relationship between fine PM and BC for each site, for correlation analysis between BC and PM was carried out for PM sizes less than $0.9 \mu\text{m}$ for each glacier studied compared to the city of Santiago which results can be observed in Figure S5.

Figure S5 shows that for OAG there was a significant correlation ($R^2 > 0.6$, $p < 0.05$) between BC and particles up to $0.675 \mu\text{m}$, while in BG that there was no significant correlation ($R^2 < 0.6$) between BC and fine particles. A correlation coefficient between BC and fine particles >0.6 indicates a common and close source for both pollutants, in this case, a combustion source of BC, since particles do not yet undergo significant processes of nucleation and condensation, affecting its growth, this case was found in OAG. In the case of Santiago, there was a significant correlation ($R^2 > 0.6$) between BC and particles only in the finest size capable of measuring with our instrument ($0.265 \mu\text{m}$), indicating that the BC observed in Santiago was mainly associated with ultrafine particles (mobile sources) directly emitted from combustion sources, meanwhile, in both glaciers there was no such relationship, reinforcing the antecedents that would indicate that emissions from Santiago City would not be reaching to two glaciers.

Finally, to determine if the air masses originated in Santiago City, and therefore the PM, BC, and metal emissions released on it could reach the studied glaciers, the Hybrid Single-Particle Lagrangian Integrated Trajectory Model (HYSPLIT)⁴² was used. Figures S7 and S8 present the

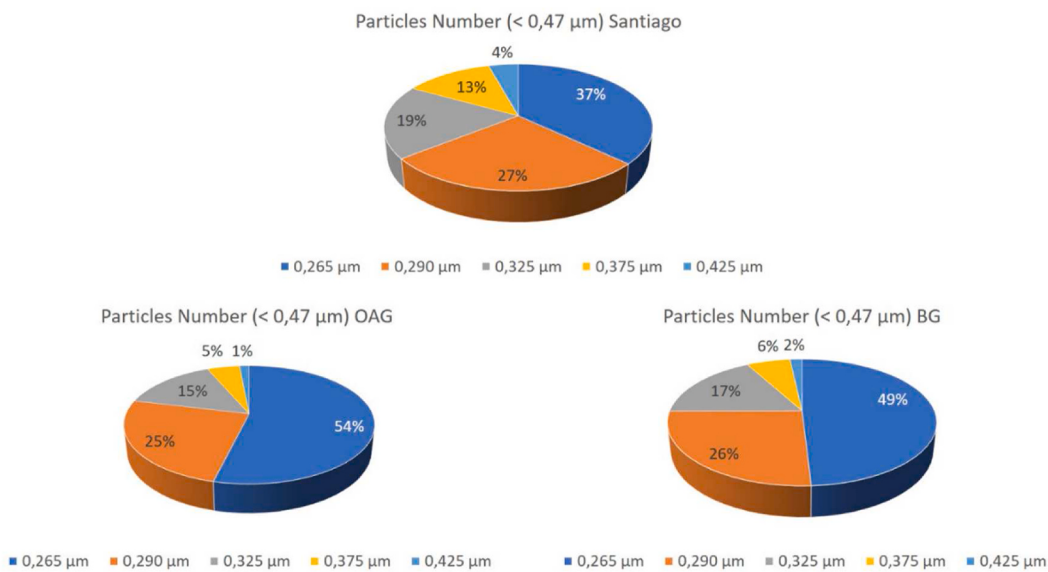


Fig. 7. Fine particles size proportions Santiago v/s OAG and BG.

plotted forward air mass trajectories for dates of measurements. In none of the studied days, the air masses generated in Santiago reached the glaciers, not even when the highest levels of atmospheric BC were demonstrated (Fig. 8), confirming that long-range transport from the city was not a significant contribution to the measured levels of

atmospheric pollutants in the studied glaciers. Those air masses did not easily reach the peaks of the Andes (Figures S9 and S10) due mainly to the great difference in terrain height (from 500 m. a.s.l in Santiago to over 4500 m. a.s.l in the mountain peaks) and especially to the low height of the mixed layer of Santiago, which in winter is barely 300 m and in summer it can reach 1000 m at most (Undurraga, 2010). Therefore, the probability that pollutants reach the free atmosphere and are transported to the mountain on the same day is unlikely, as has been proved in other studies (Cordova et al., 2016; Lapere et al., 2021).

This work presented novel measurements of major air pollutants emitted by anthropogenic activities that enhanced glacier retreat in the ChiCA though a short-term field measurement was conducted. Climate change and glacier dynamics have already been studied and it has been concluded that they cannot explain the larger glacier retreat of OAG. Moreover, BG and OAG belong to the same basin, they have similar characteristics in terms of location, area, altitude, and climate, but OAG has shown a larger retreat and mass loss in the recent decades. Glacier area decrease was calculated, -27.6% for OAG vs. -5.1% for BG between 2004 and 2014. Meanwhile, glacier mass loss of OAG almost double BG values between 2000 and 2018 was ($-0.8 \text{ m w. e. a}^{-1}$ and $-0.4 \text{ m w. e. a}^{-1}$ for OAG and BG, respectively). OAG presented a significantly higher anthropogenic impact than BG, reflected by higher levels of atmospheric BC, metals, higher correlation coefficients between atmospheric BC and fine particles, and lower albedo values. Additionally, dust concentration in the OAG snow was 67 times higher than that found in BG and BC concentration was higher in the OAG than in BG, which clearly show the impact of these LAPs on the albedo of the OAG. In agreement with these findings, the HYSPLIT analysis discards that aerosol produced in Santiago de Chile could reach the studied glaciers being the source of the anthropogenic atmospheric pollutants and dust over OAG. Meanwhile, the higher EF that OAG presented for Cu and As, elements known as specific tracers of copper mining activities, and the high correlation between BC in the air and the number of fine particles point out that activities related to nearby mines are significantly influencing OAG surface mass balance. This hypothesis is reinforced by the more negative glacier mass balance observed in the glaciers closest to the mine against those far away. Furthermore, this analysis showed that, except for those closest to mine than OAG, it has shrinkage more than other glaciers in the study area, including BG, mainly due to the more extensive influence the mining activity has had on its surroundings.

Finally, taking into account the aforementioned evidence and

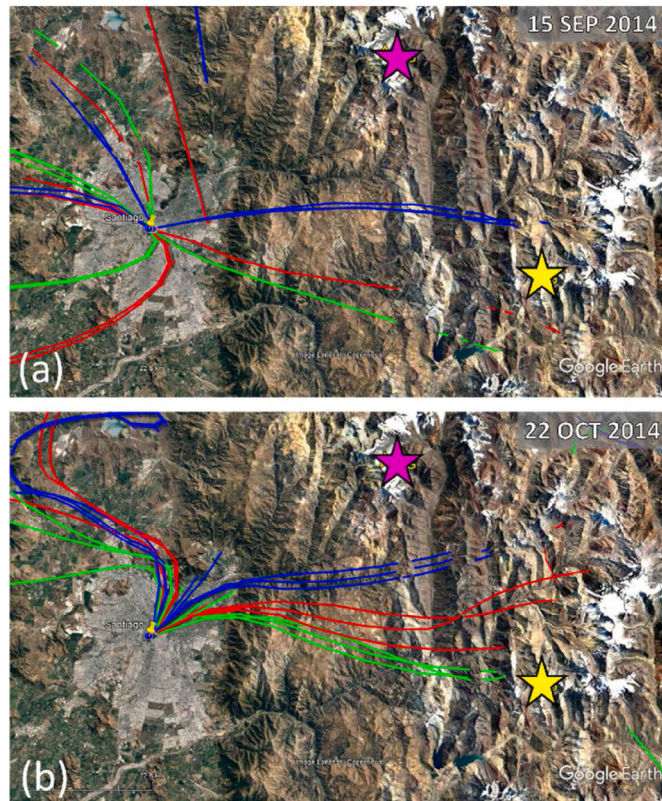


Fig. 8. Forward 24 h trajectory originated in Santiago City, obtained using the HYSPLIT model, for the two dates with the highest BC atmospheric concentrations demonstrated at (a) BG and (b) OAG. Trajectories of different starting heights are shown in different line colors. The pink star represents OAG location and yellow star BG location. Maps data: Google. (For interpretation of the references to color in this figure legend, the reader is referred to the Web version of this article.)

comparing the loss of mass of both glaciers during the period 2004–2014, it could be estimated that for the study period of the 10 years analyzed, the impact on glacial retreat due to mining in the OAG most likely corresponds to 82% of the total, and only the remaining 18% would correspond to the effect of climate change (Section S8), highlighting the importance of the impact of local pollution in the melting of glaciers in this area of the Andes and its impact on water resources.

Credit author statement

Francisco Cereceda-Balic: Conceptualization, Methodology, Investigation, Project administration, Funding acquisition, Supervision, Writing – original draft. **María Florencia Ruggeri:** Methodology, Investigation, Software, Writing – original draft. Victor Vidal: Investigation, Resources, Writing – original draft. **Lucas Ruiz:** Investigation, Software, Writing – original draft. **Joshua Fu:** Conceptualization, Writing – original draft.

Author contributions

The manuscript was written through contributions of all authors. **F.C.B** and **J.S.F** designed the study. **F.C.B** and **V.V** did the field work. **F.C.B**, **V.V** and **M.F.R** performed the data analysis and the lab work. **M.F.R** and **L.R.** performed the analysis of glacier area and mass balance variations. **F.C.B**, **V.V** and **M.F.R** led the writing of the original draft, and all the authors participated in the review and edition of it.

Declaration of competing interest

The authors declare that they have no known competing financial interests or personal relationships that could have appeared to influence the work reported in this paper.

Acknowledgment

This work has been supported by Fondef-ANIDProject ID19I10359, ANID-ANILLOACT210021, ANID-FONDECYT Regular 1221526, ANID-FONDECYT Postdoctoral Project N°3190513, , ANID-FONDECYT de Iniciación 11220525, ANID-FOVI210064 and Ministerio de Obras Públicas, Dirección General de Aguas, Unidad Glaciología y Nieves, S.I.T. N° 351, 2014, Government of Chile.

The authors acknowledge United States Geological Survey (USGS) for the satellite imagery from Landsat 5 and Landsat 8. Landsat imagery is available at <https://earthexplorer.usgs.gov/>. ASTER images are courtesy of NASA/METI/AIST/Japan Space systems and the US/Japan ASTER Science Team. The contributions of Dr. Hans Moosmüller (DRI, USA) to the discussion of aspects related to the optical properties of LAPs, are greatly appreciated.

Appendix A. Supplementary data

Supplementary data related to this article can be found at <https://doi.org/10.1016/j.envres.2022.113756>.

References

- Aamaas, B., Bøggild, C.E., Stordal, F., Berntsen, T., Holmén, K., Ström, J., 2011. Elemental carbon deposition to Svalbard snow from Norwegian settlements and long-range transport. *Tellus Ser. B Chem. Phys. Meteorol.* 63, 340–351. <https://doi.org/10.1111/j.1600-0889.2011.00531.x>.
- Arenson, L., Jakob, M., Wainstein, P., 2015. Effects of dust deposition on glacier ablation and runoff at the pascua-Lama mining Project, Chile and Argentina. In: Engineering Geology for Society and Territory - Volume 1: Climate Change and Engineering Geology. Springer International Publishing, pp. 27–31. <https://doi.org/10.1007/978-3-319-09300-0>.
- Ayala, A., Farfás-barahona, D., Huss, M., Pellicciotti, F., McPhee, J., 2020. Glacier runoff variations since 1955 in the Maipo river basin, in the semiarid Andes of central Chile. *Cryosphere* 14, 2005–2027. <https://doi.org/10.5194/tc-14-2005-2020>.
- Ayala, A., Pellicciotti, F., MacDonell, S., McPhee, J., Vivero, S., Campos, C., Egli, P., 2016. Modelling the hydrological response of debris-free and debris-covered glaciers to present climatic conditions in the semiarid Andes of central Chile. *Hydrol. Process.* 30, 4036–4058. <https://doi.org/10.1002/hyp.10971>.
- Baraza, G., Nussbaumer, S.U., Tapia, G., Valdés, J., García, J.L., Videla, Y., Albornoz, A., Arias, V., 2017. Glacier inventory and recent glacier variations in the Andes of Chile, South America. *Ann. Glaciol.* 58, 166–180. <https://doi.org/10.1017/aog.2017.28>.
- Bellisario, A., Ferrando, F., Janke, J., 2013. Recursos hídricos en Chile: La relación crítica entre los glaciares y la minería para el manejo sustentable del agua. *Invest. Geográficas* 46, 3–24. <https://doi.org/10.5354/0719-5370.2014.30288>.
- Berthier, E., Arnaud, Y., Baratoux, D., Vincent, C., Re, F., 2004. Recent rapid thinning of the “Mer de Glace” glacier derived from satellite optical images. *Geophys. Res. Lett.* 31, 2–5. <https://doi.org/10.1029/2004GL020706>.
- Boisier, J.P., Rondanelli, R., Garreaud, R., Muñoz, F., 2016. Anthropogenic contribution to the southeast pacific precipitation decline and recent (2010–2015) mega-drought in Chile. In: Am. Geophys. Union, Fall Meet. 2015. <https://doi.org/10.1002/2015GL067265.Abstract>. Abstr. id. H43E-1549 43, 1–9.
- Bolaño-Ortiz, T.R., Pascual-Flores, R.M., López-Noreña, A.I., Ruggeri, M.F., Lakkis, S.G., Fernández, R.P., Pulaifito, S.E., 2019. Assessment of absorbing aerosols on austral spring snow albedo reduction by several basins in the Central Andes of Chile from daily satellite observations (2000–2016) and a case study with the WRF-Chem model. *SN Appl. Sci.* 1, 1–13. <https://doi.org/10.1007/s42452-019-1256-z>.
- Bond, T.C., Doherty, S.J., Fahey, D.W., Forster, P.M., Berntsen, T., DeAngelo, B.J., Flanner, M.G., Ghan, S., Kärcher, B., Koch, D., Kinne, S., Kondo, Y., Quinn, P.K., Sarofim, M.C., Schultz, M.G., Schulz, M., Venkataraman, C., Zhang, H., Zhang, S., Bellouin, N., Guttikunda, S.K., Hopke, P.K., Jacobson, M.Z., Kaiser, J.W., Klimont, Z., Lohmann, U., Schwarz, J.P., Shindell, D., Storelvmo, T., Warren, S.G., Zender, C.S., 2013. Bounding the role of black carbon in the climate system: a scientific assessment. *J. Geophys. Res. Atmos.* 118, 5380–5552. <https://doi.org/10.1002/jgrd.50171>.
- Burger, F., Ayala, A., Farias, D., Shaw, T.E., MacDonell, S., Brock, B., McPhee, J., Pellicciotti, F., 2019. Interannual variability in glacier contribution to runoff from a high-elevation Andean catchment: understanding the role of debris cover in glacier hydrology. *Hydrol. Process.* 33, 214–229. <https://doi.org/10.1002/hyp.13354>.
- Casey, K.A., Kaspari, S.D., Skiles, S.M., Kreutz, K., Handley, M.J., 2017. The spectral and chemical measurement of pollutants on snow near South Pole, Antarctica. *J. Geophys. Res.* 122, 6592–6610. <https://doi.org/10.1002/2016JD026418>.
- Cereceda-Balic, F., Gorená, T., Soto, C., Vidal, V., Lapuerta, M., Moosmüller, H., 2019. Optical determination of black carbon mass concentrations in snow samples: a new analytical method. *Sci. Total Environ.* 697, 133934. <https://doi.org/10.1016/j.scitotenv.2019.133934>.
- Cereceda-Balic, F., Palomo-marín, M.R., Bernalte, E., Vidal, V., Christie, J., Fadic, X., Guevara, J.L., Miro, C., Gil, E.P., 2012. Impact of Santiago de Chile urban atmospheric pollution on anthropogenic trace elements enrichment in snow precipitation at Cerro Colorado, Central Andes. *Atmos. Environ.* 47, 51–57. <https://doi.org/10.1016/j.atmosenv.2011.11.045>.
- Cereceda-Balic, F., Ruggeri, M.F., Vidal, V., 2020. glacier retreat differences in Chilean central Andes and their relation with anthropogenic black carbon pollution. In: 2020 IEEE Latin American GRSS & ISPRS Remote Sensing Conference (LAGIRS). IEEE, Santiago de Chile, pp. 434–440. <https://doi.org/10.1109/LAGIRS48042.2020.9165676>.
- Cereceda-Balic, F., Vidal, V., Moosmüller, H., Lapuerta, M., 2018. Reduction of snow albedo from vehicle emissions at Portillo, Chile. *Cold Reg. Sci. Technol.* 146, 43–52. <https://doi.org/10.1016/j.coldregions.2017.11.008>.
- Cordova, A.M., Arévalo, J., Marín, J.C., Baumgardner, D., Raga, G.B., Pozo, D., Ochoa, C. A., Rondanelli, R., 2016. On the transport of urban pollution in an Andean mountain valley. *Aerosol Air Qual. Res.* 16, 593–605. <https://doi.org/10.4209/aaqr.2015.05.0371>.
- De Gregori, I., Fuentes, E., Rojas, M., Pinochet, H., Potin-Gautier, M., 2003. Monitoring of copper, arsenic and antimony levels in agricultural soils impacted and non-impacted by mining activities, from three regions in Chile. *J. Environ. Monit.* 5, 287–295. <https://doi.org/10.1039/b211469k>.
- DGA, 2010. Balance de masa en el glaciar Echaurren Norte temporadas 1997–1998 a 2008–2009, vol. 32. Dir. Gen. Aguas.
- Dirección General de Aguas, 2011. Variaciones recientes de Glaciares en Chile, según principales zonas glaciológicas. Informe final.
- Doherty, S.J., Warren, S.G., Grenfell, T.C., Clarke, A.D., Brandt, R.E., 2010. Light-absorbing impurities in Arctic snow. *Atmos. Chem. Phys.* 10, 11647–11680. <https://doi.org/10.5194/acp-10-11647-2010>.
- Dumont, M., Brun, E., Picard, G., Michou, M., Libois, Q., Petit, J.R., Geyer, M., Morin, S., Josse, B., 2014. Contribution of light-absorbing impurities in snow to Greenland's darkening since 2009. *Nat. Geosci.* 7, 509–512. <https://doi.org/10.1038/ngeo2180>.
- Dussaillant, I., Berthier, E., Brun, F., Masiokas, M., Hugonnet, R., Favier, V., Rabatel, A., Pitté, P., Ruiz, L., 2019. Two decades of glacier mass loss along the Andes. *Nat. Geosci.* 12, 802–808. <https://doi.org/10.1038/s41561-019-0432-5>.
- Espizua, L., Bengoechea, J.D., 1990. Surge of grande del Nevado Glacier (mendoza, Argentina) in 1984 : its evolution through satellite images. *Geogr. Ann.* 72, 255–259. <https://doi.org/10.2307/521153>.
- Farfás-Barahona, D., Ayala, Á., Bravo, C., Vivero, S., Seehaus, T., Vijay, S., Schaefer, M., Buglio, F., Casassa, G., Braun, M., 2020. 60 Years of glacier elevation and mass changes in the Maipo river basin, central Andes of Chile. *Rem. Sens.* 12, 1–19. <https://doi.org/10.3390/rs12101658>.
- Farfás-Barahona, D., Vivero, S., Casassa, G., Schaefer, M., Burger, F., Seehaus, T., Iribarren-Anacona, P., Escobar, F., Braun, M.H., 2019. Geodetic mass balances and area changes of echaurren Norte glacier (central Andes, Chile) between 1955 and 2015. *Rem. Sens.* 11 <https://doi.org/10.3390/rs11030260>.

- Garreaud, R.D., Boisier, J.P., Rondanelli, R., Montecinos, A., Sepúlveda, H.H., Veloso-Aguila, D., 2020. The Central Chile Mega Drought (2010–2018): a climate dynamics perspective. *Int. J. Climatol.* 40, 421–439. <https://doi.org/10.1002/joc.6219>.
- Grange, S.K., 2015. Technical Note: Averaging Wind Speeds and Directions. <https://doi.org/10.13140/RG.2.1.3349.2006>. Auckland.
- Hadley, O.L., Kirschstetter, T.W., 2012. Black-carbon reduction of snow albedo. *Nat. Clim. Chang.* 2, 437–440. <https://doi.org/10.1038/nclimate1433>.
- Huss, M., 2013. Density assumptions for converting geodetic glacier volume change to mass change. *Cryosphere* 877–887. <https://doi.org/10.5194/tc-8-877-2013>.
- Jeffries, D.S., 1990. Snowpack storage of pollutants, release during melting, and impact on receiving waters. In: *Acidic Precipitation*. Springer-Verlag, New York.
- Lai, A.M., Shafer, M.M., Dibb, J.E., Polashenski, C.M., Schauer, J.J., 2017. Elements and inorganic ions as source tracers in recent Greenland snow. *Atmos. Environ.* 164, 205–215. <https://doi.org/10.1016/j.atmosenv.2017.05.048>.
- LaPere, R., Mailler, S., Menut, L., Huneeus, N., 2021. Pathways for wintertime deposition of anthropogenic light-absorbing particles on the Central Andes cryosphere. *Environ. Pollut.* 272, 115901. <https://doi.org/10.1016/j.envpol.2020.115901>.
- Malmros, J.K., Mernild, S.H., Wilson, R., Tagesson, T., 2018. Snow cover and snow albedo changes in the central Andes of Chile and Argentina from daily MODIS observations (2000 – 2016). *Remote Sens. Environ.* 209, 240–252. <https://doi.org/10.1016/j.rse.2018.02.072>.
- Malmros, J.K., Mernild, S.H., Wilson, R., Yde, J.C., Fensholt, R., 2016. Glacier area changes in the central Chilean and Argentinean Andes 1955–2013/14. *J. Glaciol.* 62, 391–401. <https://doi.org/10.1017/jog.2016.43>.
- Man, Q.X., Guo, H.D., Liu, G., Dong, P.L., 2014. Comparison of different methods for monitoring glacier changes observed by Landsat images. *IOP Conf. Ser. Earth Environ. Sci.* 17, 1–6. <https://doi.org/10.1088/1755-1315/17/1/012127>.
- Masiokas, M.H., Rabatel, A., Rivera, A., Ruiz, L., Pitte, P., Ceballos, J.L., Barcaza, G., Soruco, A., Bown, F., Berthier, E., Dussaillant, I., MacDonell, S., 2020. A review of the current state and recent changes of the andean cryosphere. *Front. Earth Sci.* 8. <https://doi.org/10.3389/feart.2020.00099>.
- Molina, L.T., Gallardo, L., Andrade, M., Baumgardner, D., Borbor-Córdova, M., Bórquez, R., Casassa, G., Cereceda-Balic, F., Dawidowski, L., Garreaud, R., Huneeus, N., Lambert, F., McCarty, J., Mc Phee, J., Mena-Carrasco, M., Raga, G., Schmitt, C., Schwarz, J., 2015. Pollution and its impacts on the south American cryosphere. *Earth's Futur.* 3, 345–369. <https://doi.org/10.1002/2015EF000311>.
- Oerlemans, J., van Pelt, W.J.J., 2015. A model study of Abrahamsenbreen, a surging glacier in northern Spitsbergen. *Cryosphere* 9, 767–779. <https://doi.org/10.5194/tc-9-767-2015>.
- Paul, F., Barrand, N.E., Baumann, S., Berthier, E., Bolch, T., Casey, K., Frey, H., Joshi, S., Ponomarov, V., Le Bris, R., Mölg, N., Nosenko, G., Nutt, C., Pope, A., Racoviteanu, A., Rastner, P., Raup, B., Schärer, K., Steffen, S., Winsvold, S., 2013. On the accuracy of glacier outlines derived from remote-sensing data. *Ann. Glaciol.* 54, 171–182. <https://doi.org/10.3189/2013AoG63A296>.
- Petzold, A., Ogren, J.A., Fiebig, M., Laj, P., Li, S.M., Baltensperger, U., Holzer-Popp, T., Kinne, S., Pappalardo, G., Sugimoto, N., Wehrli, C., Wiedensohler, A., Zhang, X.Y., 2013. Recommendations for reporting black carbon measurements. *Atmos. Chem. Phys.* 13, 8365–8379. <https://doi.org/10.5194/acp-13-8365-2013>.
- Pitte, P., Berthier, E., Masiokas, M.H., Cabot, V., Ruiz, L., Hidalgo, L.F., Gargantini, H., Zalazar, L., 2016. Geometric evolution of the horcones inferior glacier (mount aconcagua, central Andes) during the 2002–2006 surge. *J. Geophys. Res. Earth Surf.* 111–127. <https://doi.org/10.1002/2015JF003522>.
- Qu, B., Ming, J., Kang, S.-C., Zhang, G.-S., Li, Y.-W., Li, C.-D., Zhao, S.-Y., Ji, Z.-M., Cao, J.-J., 2014. The decreasing albedo of Zhadang glacier on western Nyainqntanglha and the role of light-absorbing impurities. *Atmos. Chem. Phys. Discuss.* 14, 13109–13131. <https://doi.org/10.5194/acpd-14-13109-2014>.
- Riggs, G., Hall, D., Salomonson, V., 1994. A snow Index for the Landsat thematic mapper and moderate resolution imaging spectroradiometer. In: *Proceedings of IGARSS 1994: IEEE International Geoscience and Remote Sensing Symposium*. Pasadena, California, pp. 1942–1944. <https://doi.org/10.1109/IGARSS.1994.399618>.
- Rowe, P.M., Cordero, R.R., Warren, S.G., Stewart, E., Doherty, S.J., Pankow, A., Schrempp, M., Casassa, G., Carrasco, J., Pizarro, J., MacDonell, S., Damiani, A., Lambert, F., Rondanelli, R., Huneeus, N., Fernandoy, F., Neshyba, S., 2019. Black carbon and other light-absorbing impurities in snow in the Chilean Andes. *Sci. Rep.* 9, 1–16. <https://doi.org/10.1038/s41598-019-39312-0>.
- Ruiz, L., Berthier, E., Viale, M., Pitte, P., Masiokas, M.H., 2017. Recent geodetic mass balance of Monte Tronador glaciers, northern Patagonian Andes. *Cryosphere* 619–634. <https://doi.org/10.5194/tc-11-619-2017>.
- Ruiz Pereira, S.F., Veettil, B.K., 2019. Glacier decline in the Central Andes (33°S): context and magnitude from satellite and historical data. *J. South Am. Earth Sci.* 94, 102249. <https://doi.org/10.1016/j.jsames.2019.102249>.
- Shaw, T.E., Ulloa, G., Fariás-Barahona, D., Fernandez, R., Lattus, J.M., McPhee, J., 2020. Glacier albedo reduction and drought effects in the extratropical Andes, 1986–2020. *J. Glaciol.* 67 (261), 158–169. <https://doi.org/10.1017/jog.2020.102>.
- Skiles, S.M.K., Painter, T., 2017. Daily evolution in dust and black carbon content, snow grain size, and snow albedo during snowmelt, Rocky Mountains, Colorado. *J. Glaciol.* 63, 118–132. <https://doi.org/10.1017/jog.2016.125>.
- Stehlik, M., Hermann, P., Torres, S., Kisel'ák, J., Rivera, A., 2017. On dynamics underlying variance of mass balance estimation in Chilean glaciers. *Ecol. Complex.* 31, 149–164. <https://doi.org/10.1016/j.ecocom.2017.06.008>.
- Tuzet, F., Dumont, M., Picard, G., Lamare, M., Voisin, D., Nabat, P., Lafayesse, M., Larue, F., Revuelto, J., Arnaud, L., 2020. Quantification of the radiative impact of light-absorbing particles during two contrasted snow seasons at Col du Lautaret (2058 m a.s.l., French Alps). *Cryosphere Discuss.* 1–38. <https://doi.org/10.5194/tc-2019-287>.
- Undurraga, A.A., 2010. Desarrollo de capa de mezcla en Santiago: Análisis observacional y comparación con modelo de mesoscala. Universidad de Chile.
- Vicuña, S., Garreaud, R.D., McPhee, J., 2011. Climate change impacts on the hydrology of a snowmelt driven basin in semiarid Chile. *Clim. Change* 105, 469–488. <https://doi.org/10.1007/s10584-010-9888-4>.
- Yasunari, T.J., Tan, Q., Lau, K.-M., Bonasoni, P., Marinoni, A., Laj, P., Ménégoz, M., Takemura, T., Chin, M., 2013. Estimated range of black carbon dry deposition and the related snow albedo reduction over Himalayan glaciers during dry pre-monsoon periods. *Atmos. Environ.* 78, 259–267. <https://doi.org/10.1016/j.atmosenv.2012.03.031>.
- Zalazar, L., Ferri, L., Castro, M., Gargantini, H., Gimenez, M., Pitte, P., Ruiz, L., Masiokas, M., Villalba, R., 2017. Glaciares de Argentina : resultados Preliminares del Inventario Nacional de Glaciares Glaciers of Argentina : preliminary Results of the National Inventory of Glaciers. *Rev. Glaciares y ecosistemas montaña* 2, 13–22. <https://doi.org/10.36580/rgem.i2.13-22>.
- Zdanowicz, C., Zheng, J., Klimenko, E., Outridge, P.M., 2017. Mercury and other trace metals in the seasonal snowpack across the subarctic taiga-tundra ecotone, Northwest Territories, Canada. *Appl. Geochem.* 82, 63–78. <https://doi.org/10.1016/j.apgeochem.2017.04.011>.
- Zhang, Y., Kang, S., Li, C., Gao, T., Cong, Z., Sprenger, M., Liu, Y., Li, X., Guo, J., Sillanpää, M., Wang, K., Chen, J., Li, Y., Sun, S., 2017. Characteristics of black carbon in snow from Laohugou No. 12 glacier on the northern Tibetan Plateau. *Sci. Total Environ.* 607–608, 1237–1249. <https://doi.org/10.1016/j.scitotenv.2017.07.100>.